Letter

Constraining ultralight dark matter using the Fermi-LAT pulsar timing array

Zi-Qing Xia,[1] Tian-Peng Tang,[1,2] Xiaoyuan Huang,[1,2,*] Qiang Yuan,[1,2,†] and Yi-Zhong Fan[1,2,‡]

[1]*Key Laboratory of DM and Space Astronomy, Purple Mountain Observatory, Chinese Academy of Sciences, Nanjing 210033, China*

[2]*School of Astronomy and Space Science, University of Science and Technology of China, Hefei, Anhui 230026, China*

(Received 11 April 2023; accepted 22 May 2023; published 28 June 2023)

Ultralight dark matter (ULDM) is proposed as a theoretical candidate of dark matter particles with masses of approximately 10^{-22} eV. The interactions between ULDM particles and standard model particles would cause variations in pulse arrival times of millisecond pulsars, which means that the pulsar timing array (PTA) can be used to indirectly detect ULDM. In this Letter, we use the gamma-ray PTA composed of 29 millisecond pulsars observed by the *Fermi* Large Area Telescope (Fermi-LAT) to test four ULDM effects, including gravitational effects for generalized ULDM with different spin-0/1, the fifth-force coupling effect of dark photons, and the modified gravitational effect of the spin-2 ULDM. The gamma-ray pulsar timing is not affected by the ionized interstellar medium and suffers relatively simple noises, unlike that of the radio band. Our work is the first time that the gamma-ray PTA has been used to search for the ULDM. No significant signals of ULDM are found based on the Fermi-LAT PTA for all four kinds of ULDM models. Constraints on ULDM parameters are set with the 95% confidence level, which provides a complementary check of the nondetection of ULDM for radio PTAs and direct detection experiments.

DOI: 10.1103/PhysRevD.107.L121302

I. INTRODUCTION

Dark matter (DM) is believed to make up almost a quarter of the total energy of the current Universe, which is more than 5 times of ordinary visible matter [1]. Theoretical physicists have proposed various hypothetical particles as dark matter candidates, such as weakly interacting massive particles [2], axions [3], sterile neutrinos [4], and dark photons [5]. The masses of these proposed dark matter particles span a broad range from below 10^{-22} eV to above TeV.

Here, we focus on the ultralight dark matter (ULDM) with the mass of $\sim 10^{-22}$ eV, whose de Broglie wavelength is up to the sub-Galactic scale ($\sim$1 kpc). Compared with other dark matter candidates, ULDM have the advantage in forecasting small-scale structures consistent with observations [6–13]. ULDM models can be roughly classified by the spin of the particle: (1) the spin-0 (scalar or pseudoscalar) ULDM case, like ultralight axionlike scalar field dark matter [14–18]; (2) the spin-1 (vector) ULDM case, especially ultralight dark photons (DPs) [19–23]; and (3) the spin-2 (tensor) ULDM case [24–26]. Because of the macroscopic de Broglie wavelength, the gravitational effect of generalized spin-0/1 ULDM and the coupling effect (usually dubbed as the fifth force) of dark photons with spin-1 would cause oscillations of Earth and pulsars. For the spin-2 ULDM, photons propagating from pulsars to Earth would be affected by the modified gravitational effect and follow the geodesics of the new metric related to the surrounding spin-2 ULDM field. These effects for all these cases would result in monochromatic periodical variations in the pulse arrival time and provide an interesting method to probe ULDM with the pulsar timing array (PTA). Though another multifield ULDM scenario has also been discussed for a wideband spectrum in Ref. [27], here we mainly focus on the monochromatic signal induced by ULDM in the nanohertz range using the PTA dataset. In addition to the PTA, Ref. [28] innovatively proposed utilizing photon ring astrometry from the Event Horizon Telescope to detect the presence of the ULDM.

The PTA experiments have been continuously monitoring a series of highly stable millisecond pulsars (MSPs) for more than a decade and accurately recording the arrival times of their periodic electromagnetic pulses. Gravitational perturbations could induce variations in the time that pulses take from a millisecond pulsar to Earth. Therefore, PTA is designed to be an excellent detector for nanohertz-frequency gravitational perturbations from the gravitational wave background (GWB) and the single gravitational wave event, and also for the oscillations induced by ULDM [29–39]. The traditional PTA projects are generally at the radio wavelength: the Parkes pulsar timing array (PPTA) in Australia [40,41], the European

*Corresponding author.
xyhuang@pmo.ac.cn
†Corresponding author.
yuanq@pmo.ac.cn
‡Corresponding author.
yzfan@pmo.ac.cn

pulsar timing array [42,43], the North American Nanohertz Observatory for Gravitational Waves [44,45], and that for the 500-m aperture spherical radio telescope [46,47]. Recently, a gamma-ray PTA has recently been constructed from the *Fermi* large area telescope (Fermi-LAT) data for searching GWB from merging supermassive black hole binaries [48], which can provide an independent and complementary check for radio PTAs. Also, the gamma-ray PTA has the advantage that it would not involve the uncertainty from the effect of the ionized interstellar medium (IISM) on the propagating path of photons, which can induce additional noises in radio PTAs. In this Letter, the public timing data of the Fermi-LAT PTA[1] are adopted to search for the signals produced by the coherent oscillation effect of ULDM particles with different spin,[2] including the gravitational effects for the spin-0/1 ULDM, the fifth-force effect of spin-1 dark photons, and the modified gravitational effect for the spin-2 ULDM.

In this Letter, the amplitude of the ULDM field is assumed to be proportional to the local density of dark matter ($\rho_{\rm DM}$) or its square root (except for the fifth-force case). Considering that measurement time is much shorter than coherence time ($\tau_c \sim 10^6/f$, where f is the frequency of the oscillating ULDM field), the amplitude is random following a distribution rather than the deterministic relation [50–52]. This *stochastic* treatment will result in a change of the final results on, e.g., the coupling between ULDM and the standard model field, by a factor of 1–10 compared with the *deterministic* treatment [51,52]. Here, for the convenience of comparison with previous works [32,34,36] based on the radio PTA, we keep the deterministic treatment for most cases, except for the fifth-force signal of the dark photon, in which the stochastic distribution of the amplitude is taken into account [35]. The effect due to the stochastic nature of the ULDM field will be explored in detail in future works. It is expected that similar impacts on the radio and gamma-ray PTAs will be obtained when considering the stochastic distribution of the ULDM amplitude in the Bayesian inference.

II. ULTRALIGHT DARK MATTER MODEL

In our Letter, we focus on four ULDM effects: the gravitational effects for ULDM with spin-0/1, the fifth-force effect of dark photons, and the modified gravitational effect of the spin-2 ULDM. The detailed descriptions of signals for these four effects are shown in the Supplemental Material, Sec. I [53]. For the spin-0 gravitational signal, the ULDM would induce oscillations of Earth and pulsars and cause periodical residuals in times of arrival (TOA) of pulse, which can be written as [31,32]

$$s(t) = \frac{\Psi}{m}\sin(\theta_e - \theta_p)\cos(2mt + \theta_e + \theta_p), \quad (1)$$

where m is the mass of ULDM, and θ_e and θ_p characterize oscillation phases for Earth and pulsar terms, respectively. The oscillating amplitude Ψ depends on the density of dark matter $\rho_{\rm DM}$,

$$\Psi = \frac{G\rho_{\rm DM}}{\pi f^2} \approx 6.1\times 10^{-18}\left(\frac{m}{10^{-22}\ {\rm eV}}\right)^{-2}\left(\frac{\rho_{\rm DM}}{\rho_0}\right), \quad (2)$$

where $\rho_0 = 0.4\ {\rm GeV\,cm^{-3}}$ is the measured local dark matter density near Earth [54,55]. Different from the spin-0 case, the gravitational signal of the spin-1 ULDM would have an extra contribution from the traceless spatial metric perturbations, related to the oscillation angle θ [33,34],

$$s(t) = -\frac{3}{8}(1+2\cos 2\theta)\frac{h_{\rm osc}}{m}\sin(\theta_e-\theta_p)\cos(2mt+\theta_e+\theta_p), \quad (3)$$

where the amplitude $h_{\rm osc}$ is also dependent on $\rho_{\rm DM}$,

$$h_{\rm osc} = \frac{8\pi G\rho_{\rm DM}}{3m^2} \approx 1.7\times 10^{-17}\left(\frac{m}{10^{-22}\ {\rm eV}}\right)^{-2}\left(\frac{\rho_{\rm DM}}{\rho_0}\right). \quad (4)$$

In the case of the ultralight dark photon, its fifth force could also lead to oscillations of Earth and pulsars and induce the TOA residuals. Here we consider two new gauge interactions [$U(1)_B$ and $U(1)_{B-L}$], as shown in the Supplemental Material, Sec. I C [53]. The timing residuals caused by the "fifth-force" effect can be given by [35,56]

$$s(t)^{(B)} = \frac{\epsilon e}{m}\boldsymbol{A_0}\left[\frac{q_e^{(B)}}{m_e}\cos(mt+\boldsymbol{\theta}_e) - \frac{q_p^{(B)}}{m_p}\cos(mt+\boldsymbol{\theta}_p)\right]\cdot\boldsymbol{n}, \quad (5)$$

$$s(t)^{(B-L)} = \frac{\epsilon e}{m}\boldsymbol{A_0}\left[\frac{q_e^{(B-L)}}{m_e}\cos(mt+\boldsymbol{\theta}_e) - \frac{q_p^{(B-L)}}{m_p}\cos(mt+\boldsymbol{\theta}_p)\right]\cdot\boldsymbol{n}, \quad (6)$$

where ϵ is the coupling strength of new gauge interaction, e is the electromagnetic coupling constant, $\boldsymbol{A_0}$ is the amplitude of the dark photon field, $\boldsymbol{n}$ is the normalized position vector pointing from Earth to the pulsar, and $q_{e,p}^{(B)}$, $q_{e,p}^{(B-L)}$, and $m_{e,p}$ each represent the B number, the $B-L$ number, the mass of Earth, and the pulsar. As for the spin-2 case, its modified gravitational effect could have a significant impact on the propagation of photons from pulsars to Earth and result in the TOA residuals given by [36]

$$s(t) = \frac{\alpha\sqrt{2\rho_0}}{\sqrt{15}m^2 M_{\rm P}}\cos\left(mt + \frac{\theta_e+\theta_p}{2}\right), \quad (7)$$

where α is the dimensionless strength constant and $M_{\rm P}$ is the reduced Planck mass. Prior distributions of parameters for all four ULDM effects are summarized in Table S1 in the Supplemental Material, Sec. I [53].

[1] https://zenodo.org/record/6374291#.YzVcbC-KFpR.

[2] Recently, another work used the Fermi-LAT PTA data to study spin-0 ULDM [49].

III. THE FERMI-LAT PTA

A. Data

The Fermi-LAT Collaboration uses 12.5 yr of Fermi-LAT data from August 4, 2008 to January 28, 2021 to form the first gamma-ray PTA, also called the Fermi-LAT PTA [48]. It is composed of the 35 brightest and most stable gamma-ray MSPs. However, only 29 of 35 MSPs in the Fermi-LAT PTA can efficiently estimate TOA of pulses[3] and are suitable for the TOA-based method, which is widely used in radio PTAs.

In this Letter, we adopt the TOA-based method and use TOA data recorded in the .tim files for these 29 MSPs (as the "Full 29" set in Ref. [48]). We summarize the basic information [48,57] for each pulsar in Table S2 in the Supplemental Material, Sec. II [53].

The Fermi-LAT PTA has calculated TOA by a cadence of 2, 1.5, and 1 yr^{-1} and obtained a total of 25, 19, and 12 TOA for each pulsar. The TOA with a higher cadence can provide more high-frequency information and larger data volume. Hence, in a general way, the 2 yr^{-1} cadence is a relatively optimal choice. However, PSR J0533 + 6759, PSR J0740 + 6620, PSR J1625-0021, PSR J1939 + 2134, PSR J2034 + 3632, and PSR J2256-1024 are relatively faint in all 29 MSPs and exhibit larger systematic errors for the 2 yr^{-1} cadence than that for the longer integration [48]. For these 6 MSPs, reliable TOA produced with the 1.5 yr^{-1} cadence are adopted in the following analysis, the same as the preferred cadence used in Ref. [48].

B. Timing model

TOA of a pulsar can be reconstructed from three parts,

$$\mathrm{TOA} \sim t_{\mathrm{TM}} + \Delta t_{\mathrm{Noise}} + s(t). \tag{8}$$

The first term t_{TM} characterizes the timing model accounting for the pulsar ephemeris. In this Letter, we use the optimized ephemerides model given by Ref. [48][4] and marginalize over model uncertainties. The second term $\Delta t_{\mathrm{Noise}}$ is the timing residual contributed by noises. The third term $s(t)$ is the timing residual induced by the signal for each ULDM effect described in Sec. II. The noise parameters, signal parameters, and their prior distributions are indicated in Table S1 in the Supplemental Material, Sec. I [53].

The noises of PTA can be classified into three categories: the white (time-uncorrelated) noise (WN), the red (time-correlated) noise (RN), and the BayesEphem noise (BEph) [58], respectively,

$$\Delta t_{\mathrm{Noise}} = \Delta t_{\mathrm{WN}} + \Delta t_{\mathrm{RN}} + \Delta t_{\mathrm{BEph}}. \tag{9}$$

We describe in detail these three noise components in the Supplemental Material, Sec. III [53]. Reference [48] has made a single-pulsar noise analysis for all 29 pulsars, and the favored noise model for each pulsar is listed in Table S2 in the Supplemental Material, Sec. II [53]. For the sake of conservation, here we consider white and red noises for each pulsar and the BayesEphem noise for the PTA and marginalize over their parameters in the likelihood analysis to search for the potential ULDM signal.

IV. ANALYSIS AND RESULT

A. Data analysis

To search for the ULDM signal with the Fermi-LAT PTA, we perform the likelihood analysis for two models: the signal model (labeled as H_1) given in Eq. (8) and the null model (H_0) without timing residual contributed from the ULDM signal [$s(t)$]. The PINT software package[5] [59] and ENTERPRISE package[6] [60] are used to build the timing model of TOA and perform the likelihood analysis. Then we use the PTMCMC package[7] [61] as the stochastic sampling for posterior probabilities of parameters to obtain the best-fit values. As for the H_1 model, we repeat the analysis for each ULDM effect introduced in Sec. II, respectively. To compare models with and without signal, we take the likelihood ratio test between the H_1 and H_0 models. The likelihood ratio (λ_{LR}) can be given by [62]

$$\lambda_{\mathrm{LR}} = 2 \ln \frac{\mathcal{L}_{\max}(\mathrm{H}_1)}{\mathcal{L}_{\max}(\mathrm{H}_0)}, \tag{10}$$

where $\mathcal{L}_{\max}(\mathrm{H}_1)$ and $\mathcal{L}_{\max}(\mathrm{H}_0)$ represent the maximum likelihood values we get for H_1 and H_0, respectively. According to Wilks's theorem, the likelihood ratio [62] follows the χ^2 distribution with degrees of freedom equal to the difference in numbers of parameters for the H_1 and H_0 models.

Then we further derive upper limits on ULDM parameters for each effect, respectively. For a set of fixed ULDM mass m in the corresponding frequency f range (10^{-9}, 10^{-7} Hz), we sample posterior probabilities of ULDM parameters with the numerical marginalization for all noise (WN + RN + BEph) parameters mentioned above. When posterior probabilities in the range of $[0, x_{ul}]$ are equal to 95%, we take x_{ul} as the 95% confidence level upper limit of one ULDM parameter (x) for the fixed ULDM mass m. For completeness, we also calculated upper limits for the case

[3]Another six MSPs (PSR J0312 − 0921, PSR J0418 + 6635, PSR J1513 − 2550, PSR J1543 − 5149, PSR J1741 + 1351, and PSR J1908 + 2105) do not reach the required log-likelihood threshold in the TOA estimation and can only be analyzed with the photon-by-photon method. Note that none of these six MSPs contribute significantly to the sensitivity of the Fermi-LAT PTA. See Supplemental Material of Ref. [48] for more detail.

[4]The corresponding .par files can be found in https://zenodo.org/record/6374291#.YzVcbC-KFpR.

[5]https://github.com/nanograv/pint.

[6]https://github.com/nanograv/enterprise.

[7]https://github.com/jellis18/PTMCMCSampler.

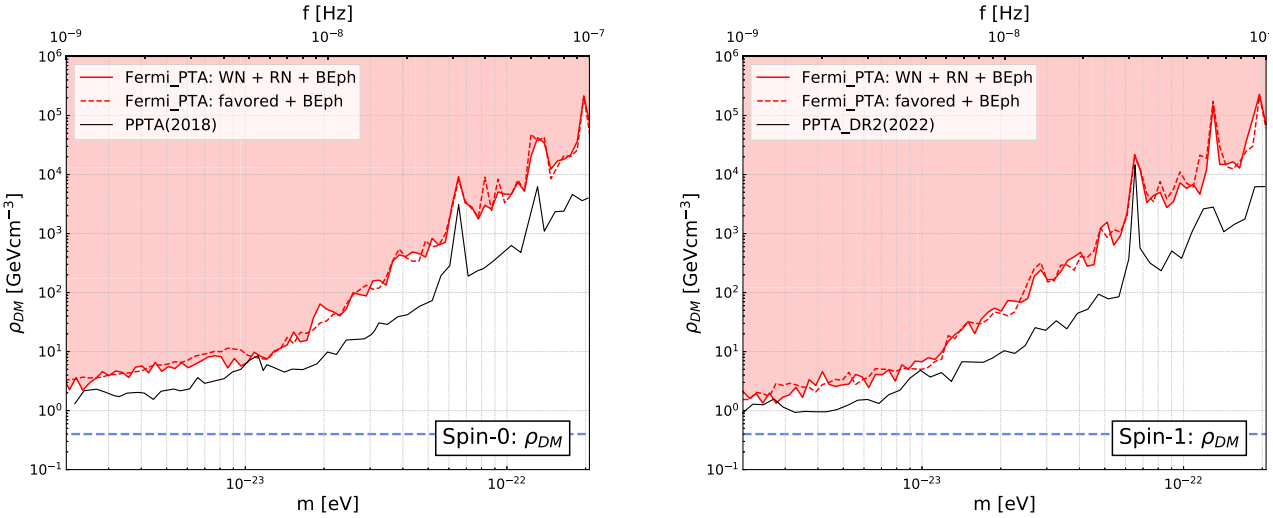

FIG. 1. Constraints on the local dark matter density $\rho_{\rm DM}$ for the spin-0/1 case with the gravitational effect. Left: the spin-0 ULDM. The black line represents upper limits from PPTA in 2018 [32]. Right: the spin-1 ULDM. The previous upper limit based on PPTA DR2 [34] is given as the black line. For both panels, red solid lines are upper limits with all noise (WN + RN + BEph) components, while red dashed lines are for the case only including the favored noise model (as listed in Table S2 in the Supplemental Material, Sec. II [53]) and the BayesEphem uncertainty (favored + BEph). The blue dashed lines are on behalf of the case in which the local dark matter density $\rho_{\rm DM}$ equals the current measurement $\rho_0 = 0.4$ GeV cm^{-3}.

only with favored noise models, as listed in Table S2 in the Supplemental Material, Sec. II [53] and the BayesEphem uncertainty, labeled as (favored + BEph).

B. Result

(i) Spin-0: Gravitational signal.—Considering the gravitational effect of the spin-0 ULDM, we get the likelihood ratio $\lambda_{\rm LR,spin-0}$ equal to 3.9 with the best-fit parameters $(m, \Psi) = (1.38 \times 10^{-24}\ \text{eV}, 1.16 \times 10^{-19})$. Considering the χ^2 distribution with 32 degrees of freedom, the corresponding statistical significance is approximately zero. Hence, the Fermi-LAT PTA shows no evidence of the gravitational signal from the spin-0 ULDM, which is consistent with the result of PPTA [32]. We calculate the 95% confidence level upper limits of oscillation amplitude Ψ for a set of fixed mass m corresponding to the frequency from 10^{-9} to 10^{-7} Hz, which are shown in the left panel of Fig. S1 in the Supplemental Material, Sec. IV [53]. According to Eq. (2), we then conduct the 95% upper limits of local dark matter density $\rho_{\rm DM}$ and exhibit them in the left panel of Fig. 1. Our constraints on the local dark matter density $\rho_{\rm DM}$ are larger than the observed local dark matter density $\rho_0 = 0.4$ GeV cm^{-3} and higher than upper limits obtained by PPTA in 2018 [32].

(ii) Spin-1: Gravitational signal.—As for the gravitational signal of the spin-1 case, the best-fit parameters are $(m, h_{\rm osc}) = (1.09 \times 10^{-23}\ \text{eV}, 6.11 \times 10^{-16})$, and the corresponding likelihood ratio is $\lambda_{\rm LR,spin-1} = 3.8$ following the χ^2 distribution with 34 degrees of freedom. Same as above, we find no significant evidence for the spin-1 gravitational signal, which is consistent with the result from PPTA DR2 [34]. The 95% confidence level upper limits with the Fermi-LAT PTA for oscillation amplitude $h_{\rm osc}$ is displayed in the right panel of Fig. S1 in the Supplemental Material, Sec. IV [53]. Conducted from Eq. (4), the upper limit of $\rho_{\rm DM}$ is shown in the right panel of Fig. 1.

(iii) Spin-1: Fifth-force signal.—In the case of the dark photon, we consider two new interaction [$U(1)_B$ and $U(1)_{B-L}$] scenarios. For the $U(1)_B/U(1)_{B-L}$ scenario, the best-fit parameters we get are $(\mathrm{m}, \epsilon) = (6.76 \times 10^{-22}\,\text{eV}, 9.95 \times 10^{-26})/(1.36 \times 10^{-22}\,\text{eV}, 5.03 \times 10^{-23})$, respectively. Corresponding likelihood ratios of $\lambda_{\rm LR,DP} = 2.1/25.2$ are asymptotically the χ^2 distribution with 37 degrees of freedom and have a statistical significance of $\sim$0. The 95% confidence level upper limits of coupling strength ϵ for the $U(1)_B$ and $U(1)_{B-L}$ scenarios are presented in the left and right panels of Fig. 2, respectively. Our constraints are found weaker than upper limits from PPTA DR2 [35]. Especially for the $U(1)_B$ scenario with masses below $\sim 7 \times 10^{-23}$ eV, we set stronger constraints than limits from the MICROSCOPE WEP experiment [63] (the horizontal black dash-dotted line in Fig. 2).

(iv) Spin-2: Modified gravitational signal.—As for the spin-2 ULDM model, we obtain the best-fit parameters as $(\mathrm{m}, \alpha) = (1.43 \times 10^{-23}\ \text{eV}, 1.45 \times 10^{-6})$ with the likelihood ratio of $\lambda_{\rm LR,spin-2} = 7.3$. Following the χ^2 distribution with 32 degrees of freedom, this likelihood ratio corresponds to a significance close to 0. The 95% confidence level upper limits of coupling strength α are further derived for a set of fixed masses of the spin-2 ULDM as shown in Fig. 3, which is also weaker than that from PPTA [36].

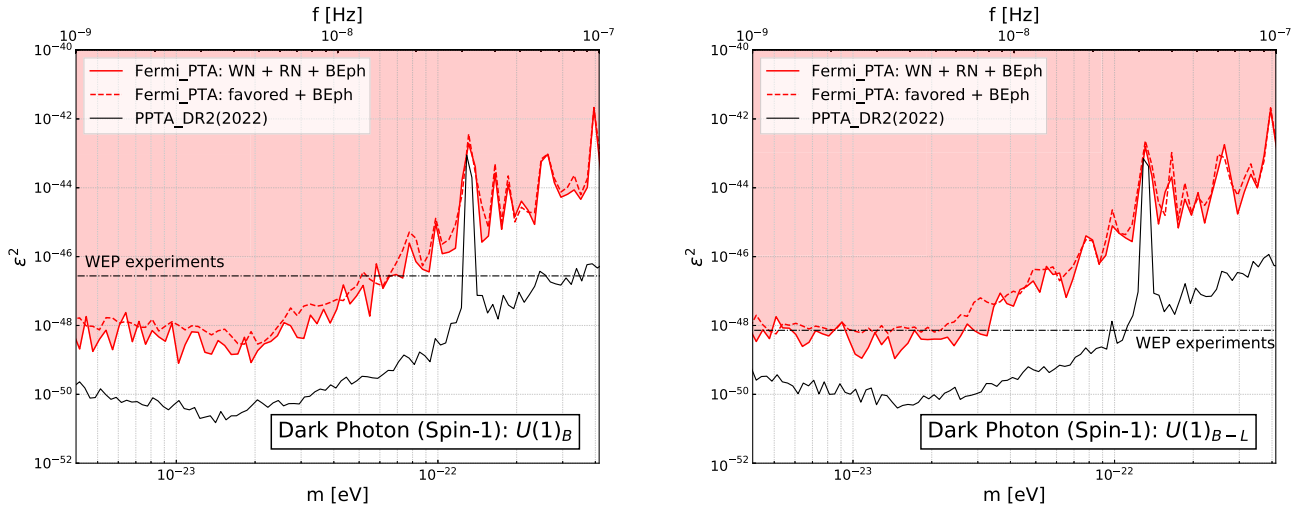

FIG. 2. Constraints on the fifth-force effect of the dark photon (spin-1) model. Left: the 95% confidence level upper limits of the coupling strength ϵ for the $U(1)_B$ scenario. Right: the $U(1)_{B-L}$ scenario. The black lines show limits based on the PPTA DR2 dataset given in Ref. [35]. The horizontal black dash-dotted lines are upper limits for the MICROSCOPE weak equivalence principle (WEP) experiment [63].

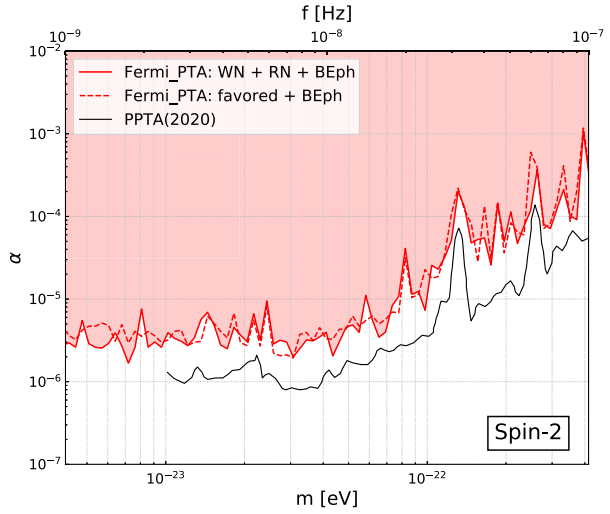

FIG. 3. The 95% confidence level upper limits of the coupling strength α for the spin-2 ULDM model. The black line indicates the upper limit set by the PPTA data in Ref. [36].

V. DISCUSSION AND SUMMARY

ULDM is a theoretical form of dark matter that consists of extremely light particles with masses of $\sim 10^{-22}$ eV beyond the standard model. PTA is a valuable tool for searching for these ULDM. The idea behind this is that the (gravitational or fifth-force) interactions between ULDM particles and standard model particles could cause slight variations in the pulse arrival times, which can be precisely measured by observing the pulsars over long periods of time.

In this Letter, we first use the gamma-ray PTA constructed from the Fermi-LAT observation of 29 MSPs to indirectly detect ULDM. Compared with the radio PTAs, the gamma-ray PTA is not affected by the turbulent IISM along the line of sight, which could induce remarkable red noises for the radio PTAs. Utilizing the traditional TOA-based method, here we search for four ULDM models, including the gravitational effects for ULDM particles with the different spin-0/1, the coupling (fifth-force) effect of dark photons, and the modified gravitational effect for the spin-2 ULDM. For all four kinds of ULDM effects, we do not find any significant signal based on the Fermi-LAT PTA dataset, which agrees with the nondetection of ULDM signals from radio PTAs and direct detection experiments. Then we further set limits on parameters of ULDM with the 95% confidence level in the corresponding frequency f range of $(10^{-9}, 10^{-7}$ Hz). As for the spin-0/1 gravitational effects, our constraints are larger than the measured local dark matter density $\rho_0 = 0.4$ GeV cm^{-3} and thus hard to further limit the particle mass of ULDM. In the case of the spin-1 dark photon effect, our constraints for the $U(1)_B$ scenario with masses below $\sim 7 \times 10^{-23}$ eV are more competitive than that of the MICROSCOPE WEP experiment. For all four effects, our limits based on the gamma-ray PTA are weaker than those of radio PTAs, due to the relatively smaller amounts of timing data. However, our work could be an independent and complementary check for the ULDM detection based on radio PTAs.

In the future, the very large gamma-ray space telescope (VLAST) [64], one of the next generation space-based gamma-ray telescopes with an effective detection area of ~ 4 m^2, will be useful to establish a stronger gamma-ray PTA to probe the ULDM and the nanohertz-frequency gravitational waves. As a very rough estimate, assuming that VLAST can detect the same number of pulsars with the same TOA precision, but enlarge the number of TOA by a factor of 5, we find that the upper limit of the oscillation amplitude Ψ will be smaller by a factor of $\sim\sqrt{5}$. Additional improvement may be achieved if the timing model and noise model can be improved given larger photon statistics, which can be explored in detail in the future.

ACKNOWLEDGMENTS

This work is supported by the National Key Research and Development Program of China (No. 2022YFF0503304), the Natural Science Foundation of China (No. 12003069, No. 11921003), the Chinese Academy of Sciences, and the Entrepreneurship and Innovation Program of Jiangsu Province.

[1] Planck Collaboration *et al.*, Planck 2015 results. XIII. Cosmological parameters, Astron. Astrophys. **594**, A13 (2016).
[2] K. Garrett and G. Dūda, Dark matter: A primer, Adv. Astron. **2011**, 968283 (2011).
[3] S. Weinberg, A New Light Boson?, Phys. Rev. Lett. **40**, 223 (1978).
[4] A. Boyarsky, M. Drewes, T. Lasserre, S. Mertens, and O. Ruchayskiy, Sterile neutrino dark matter, Prog. Part. Nucl. Phys. **104**, 1 (2019).
[5] R. Essig *et al.*, Dark sectors and new, light, weakly-coupled particles, arXiv:1311.0029.
[6] W. Hu, R. Barkana, and A. Gruzinov, Fuzzy Cold Dark Matter: The Wave Properties of Ultralight Particles, Phys. Rev. Lett. **85**, 1158 (2000).
[7] C. P. Burgess, J. P. Conlon, L.-Y. Hung, C. H. Kom, A. Maharana, and F. Quevedo, Continuous global symmetries and hyperweak interactions in string compactifications, J. High Energy Phys. 07 (**2008**) 073.
[8] M. Goodsell, J. Jaeckel, J. Redondo, and A. Ringwald, Naturally light hidden photons in LARGE volume string compactifications, J. High Energy Phys. 11 (2009) 027.
[9] M. Cicoli, M. Goodsell, J. Jaeckel, and A. Ringwald, Testing string vacua in the lab: From a hidden CMB to dark forces in flux compactifications, J. High Energy Phys. 07 (2011) 114.
[10] J. Zhang, Y.-L. Sming Tsai, J.-L. Kuo, K. Cheung, and M.-C. Chu, Ultralight axion dark matter and its impact on dark halo structure in N-body simulations, Astrophys. J. **853**, 51 (2018).
[11] J. S. Bullock and M. Boylan-Kolchin, Small-scale challenges to the ΛCDM paradigm, Annu. Rev. Astron. Astrophys. **55**, 343 (2017).
[12] E. Kendall and R. Easther, The core-cusp problem revisited: ULDM vs. CDM, Publ. Astron. Soc. Aust. **37**, e009 (2020).
[13] J. C. Niemeyer, Small-scale structure of fuzzy and axion-like dark matter, Prog. Part. Nucl. Phys. **113**, 103787 (2020).
[14] N. K. Porayko and K. A. Postnov, Constraints on ultralight scalar dark matter from pulsar timing, Phys. Rev. D **90**, 062008 (2014).
[15] L. Hui, J. P. Ostriker, S. Tremaine, and E. Witten, Ultralight scalars as cosmological dark matter, Phys. Rev. D **95**, 043541 (2017).
[16] D. Blas, D. L. Nacir, and S. Sibiryakov, Ultralight Dark Matter Resonates with Binary Pulsars, Phys. Rev. Lett. **118**, 261102 (2017).
[17] I. De Martino, T. Broadhurst, S. H. H. Tye, T. Chiueh, H.-Y. Schive, and R. Lazkoz, Recognising Axionic Dark Matter by Compton and de-Broglie Scale Modulation of Pulsar Timing, Phys. Rev. Lett. **119**, 221103 (2017).
[18] G.-W. Yuan., Z.-Q. Xia, C. Tang, Y. Zhao, Y.-F. Cai, Y. Chen, J. Shu, and Q. Yuan, Testing the ALP-photon coupling with polarization measurements of Sagittarius A*, J. Cosmol. Astropart. Phys. 03 (2021) 018.
[19] H.-K. Guo, Y. Ma, J. Shu, X. Xue, Q. Yuan, and Y. Zhao, Detecting dark photon dark matter with Gaia-like astrometry observations, J. Cosmol. Astropart. Phys. 05 (2019) 015.
[20] H. Davoudiasl and P. B. Denton, Ultralight Boson Dark Matter and Event Horizon Telescope Observations of $M87^*$, Phys. Rev. Lett. **123**, 021102 (2019).
[21] M. Fabbrichesi, E. Gabrielli, and G. Lanfranchi, *The Physics of the Dark Photon*, SpringerBriefs in Physics (Springer, Cham, 2021), 10.1007/978-3-030-62519-1.
[22] A. Caputo, A. J. Millar, C. A. J. O'Hare, and E. Vitagliano, Dark photon limits: A handbook, Phys. Rev. D **104**, 095029 (2021).
[23] G.-W. Yuan, Z.-Q. Shen, Y.-L. S. Tsai, Q. Yuan, and Y.-Z. Fan, Constraining ultralight bosonic dark matter with Keck observations of S2's orbit and kinematics, Phys. Rev. D **106**, 103024 (2022).
[24] L. Marzola, M. Raidal, and F. R. Urban, Oscillating spin-2 dark matter, Phys. Rev. D **97**, 024010 (2018).
[25] K. Aoki and K.-i. Maeda, Condensate of massive graviton and dark matter, Phys. Rev. D **97**, 044002 (2018).
[26] E. Novikov, Ultralight gravitons with tiny electric dipole moment are seeping from the vacuum, Mod. Phys. Lett. A **31**, 1650092 (2016).
[27] S. Sun, X.-Y. Yang, and Y.-L. Zhang, Pulsar timing residual induced by wideband ultralight dark matter with spin 0,1,2, Phys. Rev. D **106**, 066006 (2022).
[28] Y. Chen, X. Xue, R. Brito, and V. Cardoso, Photon Ring Astrometry for Superradiant Clouds, Phys. Rev. Lett. **130**, 111401 (2023).
[29] G. Hobbs *et al.*, The international pulsar timing array project: Using pulsars as a gravitational wave detector, Classical Quantum Gravity **27**, 084013 (2010).
[30] G. Hobbs, Pulsars as gravitational wave detectors, in *High-Energy Emission from Pulsars and their Systems*, Astrophysics and Space Science Proceedings Vol. 21 (Springer Berlin, Heidelberg, 2011), p. 229.
[31] A. Khmelnitsky and V. Rubakov, Pulsar timing signal from ultralight scalar dark matter, J. Cosmol. Astropart. Phys. 02 (2014) 019.
[32] N. K. Porayko *et al.*, Parkes pulsar timing array constraints on ultralight scalar-field dark matter, Phys. Rev. D **98**, 102002 (2018).

[33] K. Nomura, A. Ito, and J. Soda, Pulsar timing residual induced by ultralight vector dark matter, Eur. Phys. J. C **80**, 419 (2020).
[34] Y.-M. Wu *et al.*, Constraining ultralight vector dark matter with the Parkes pulsar timing array second data release, Phys. Rev. D **106**, L081101 (2022).
[35] X. Xue *et al.* (PPTA Collaboration), High-precision search for dark photon dark matter with the Parkes pulsar timing array, Phys. Rev. Res. **4**, L012022 (2022).
[36] J. M. Armaleo, D. López Nacir, and F. R. Urban, Pulsar timing array constraints on spin-2 ULDM, J. Cosmol. Astropart. Phys. 09 (2020) 031.
[37] X. Xue *et al.*, Constraining Cosmological Phase Transitions with the Parkes Pulsar Timing Array, Phys. Rev. Lett. **127**, 251303 (2021).
[38] C. Unal, F. R. Urban, and E. D. Kovetz, Probing ultralight scalar, vector and tensor dark matter with pulsar timing arrays, arXiv:2209.02741.
[39] D. E. Kaplan, A. Mitridate, and T. Trickle, Constraining fundamental constant variations from ultralight dark matter with pulsar timing arrays, Phys. Rev. D **106**, 035032 (2022).
[40] R. N. Manchester *et al.*, The Parkes pulsar timing array project, Publ. Astron. Soc. Aust. **30**, e017 (2013).
[41] M. Kerr *et al.*, The Parkes pulsar timing array project: Second data release, Publ. Astron. Soc. Aust. **37**, e020 (2020).
[42] M. Kramer and D. J. Champion, The European pulsar timing array and the large European array for pulsars, Classical Quantum Gravity **30**, 224009 (2013).
[43] G. Desvignes *et al.*, High-precision timing of 42 millisecond pulsars with the European pulsar timing array, Mon. Not. R. Astron. Soc. **458**, 3341 (2016).
[44] M. A. McLaughlin, The North American nanohertz observatory for gravitational waves, Classical Quantum Gravity **30**, 224008 (2013).
[45] Z. Arzoumanian *et al.*, The NANOGrav 12.5 yr data set: Search for an isotropic stochastic gravitational-wave background, Astrophys. J. Lett. **905**, L34 (2020).
[46] R. Nan, D. Li, C. Jin, Q. Wang, L. Zhu, W. Zhu, H. Zhang, Y. Yue, and L. Qian, The Five-Hundred Aperture Spherical Radio Telescope (FAST) project, Int. J. Mod. Phys. D **20**, 989 (2011).
[47] D. Li *et al.*, FAST in space: Considerations for a multibeam, multipurpose survey using China's 500-m aperture spherical radio telescope (FAST), IEEE Microw. Mag. **19**, 112 (2018).
[48] M. Ajello *et al.* (Fermi-LAT Collaboration), A gamma-ray pulsar timing array constrains the nanohertz gravitational wave background, Science **376**, abm3231 (2022).
[49] H. Nhan Luu, T. Liu, J. Ren, T. Broadhurst, R. Yang, J.-S. Wang, and Z. Xie, Detecting stochastic wave dark matter with Fermi-LAT γ-ray pulsar timing array, arXiv:2304.04735.
[50] J. W. Foster, N. L. Rodd, and B. R. Safdi, Revealing the dark matter halo with axion direct detection, Phys. Rev. D **97**, 123006 (2018).
[51] G. P. Centers *et al.*, Stochastic fluctuations of bosonic dark matter, Nat. Commun. **12**, 7321 (2021).
[52] A. Castillo, J. Martin-Camalich, J. Terol-Calvo, D. Blas, A. Caputo, R. T. Génova Santos, L. Sberna, M. Peel, and J. A. Rubiño-Martín, Searching for dark-matter waves with PPTA and QUIJOTE pulsar polarimetry, J. Cosmol. Astropart. Phys. 06 (2022) 014.
[53] See Supplemental Material at http://link.aps.org/supplemental/10.1103/PhysRevD.107.L121302 for the details of ULDM models and noise models, as well as some supplemental tables and figures.
[54] J. Bovy and S. Tremaine, On the local dark matter density, Astrophys. J. **756**, 89 (2012).
[55] S. Sivertsson, H. Silverwood, J. I. Read, G. Bertone, and P. Steger, The localdark matter density from SDSS-SEGUE G-dwarfs, Mon. Not. R. Astron. Soc. **478**, 1677 (2018).
[56] A. Pierce, K. Riles, and Y. Zhao, Searching for Dark Photon Dark Matter with Gravitational Wave Detectors, Phys. Rev. Lett. **121**, 061102 (2018).
[57] R. N. Manchester, G. B. Hobbs, A. Teoh, and M. Hobbs, The Australia telescope national facility pulsar catalogue, Astron. J. **129**, 1993 (2005).
[58] Z. Arzoumanian *et al.* (NANOGrav Collaboration), The NANOGrav 11-year data set: Pulsar-timing constraints on the stochastic gravitational-wave background, Astrophys. J. **859**, 47 (2018).
[59] J. Luo *et al.*, PINT: A modern software package for pulsar timing, Astrophys. J. **911**, 45 (2021).
[60] J. A. Ellis, M. Vallisneri, S. R. Taylor, and P. T. Baker, ENTERPRISE: Enhanced numerical toolbox enabling a robust pulsar inference suite (Zenodo, 2020), 10.5281/zenodo.4059815.
[61] J. Ellis and R. van Haasteren, jellis18/ptmcmcsampler: Official release (2017), 10.5281/zenodo.1037579.
[62] S. S. Wilks, The large-sample distribution of the likelihood ratio for testing composite hypotheses, Ann. Math. Stat. **9**, 60 (1938).
[63] J. Bergé, P. Brax, G. Métris, M. Pernot-Borràs, P. Touboul, and J.-P. Uzan, MICROSCOPE Mission: First Constraints on the Violation of the Weak Equivalence Principle by a Light Scalar Dilaton, Phys. Rev. Lett. **120**, 141101 (2018).
[64] Y. Z. Fan *et al.*, Very large area gamma-ray space telescope (VLAST), Acta Astron. Sin. **63**, 27 (2022).